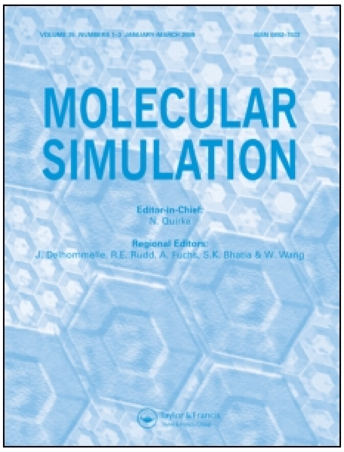

Molecular Simulation
Publication details, including instructions for authors and subscription information:
http://www.informaworld.com/smpp/title~content=t713644482

Density functional computations of Rh(I)-catalysed hydroacylation and hydrogenation of ethene using formic acid

Jigang Gao[a]; Fen Wang[b]; Qingxi Meng[a]; Ming Li[c]
[a] Department of Chemistry and Material Science, Shandong Agricultural University, Taian, People's Republic of China [b] Department of Chemistry, Taishan University, Taian, People's Republic of China [c] Department of Chemistry, Southwest-China University, Chongqing, People's Republic of China

To cite this Article Gao, Jigang , Wang, Fen , Meng, Qingxi and Li, Ming(2009) 'Density functional computations of Rh(I)-catalysed hydroacylation and hydrogenation of ethene using formic acid', Molecular Simulation, 35: 5, 419 — 427
To link to this Article: DOI: 10.1080/08927020802534843
URL: http://dx.doi.org/10.1080/08927020802534843

Molecular Simulation
Vol. 35, No. 5, April 2009, 419–427

Density functional computations of Rh(I)-catalysed hydroacylation and hydrogenation of ethene using formic acid

Jigang Gao[a], Fen Wang[b], Qingxi Meng[a]* and Ming Li[c]

[a]*Department of Chemistry and Material Science, Shandong Agricultural University, Taian, People's Republic of China;* [b]*Department of Chemistry, Taishan University, Taian, People's Republic of China;* [c]*Department of Chemistry, Southwest-China University, Chongqing, People's Republic of China*

(*Received 29 June 2008; final version received 7 October 2008*)

The rhodium-catalysed hydroacylation of alkene is one of the most useful C—H bond activation processes. The C—C bond-forming reactions via C—H bond activation have extensively been the focus of study in the fields of organic and organometallic chemistry. In this work, density functional theory has been used to study Rh(I)-catalysed hydroacylation and hydrogenation of ethene with formic acid. All the intermediates and the transition states were optimised completely at the B3LYP/6-311++G(d,p) level (LANL2DZ(d) for Rh, P). Calculation results confirm that Rh(I)-catalysed hydroacylation of ethene is exothermic and the released Gibbs free energy is −60.39 kJ/mol. Rh(I)-catalysed hydrogenation of ethene is also exothermic and the released Gibbs free energy is −150.97 kJ/mol. Rh(I)-catalysed hydroacylation of ethene is the dominant reaction mode for Rh(I)-catalysed hydroacylation and hydrogenation of ethene with formic acid. In Rh(I)-catalysed hydroacylation of ethene, the H-transfer reaction is prior to the C—C bond-forming reaction. Therefore, the reaction mode 'a' (i.e. **ca → M1 → TS1 → M2 → TS2a → M3a → TS3a → M4 → P1**) is the dominant reaction pathway for Rh(I)-catalysed hydroacylation and hydrogenation of ethene. The theoretically predicted dominant product is propane acid.

Keywords: Rh-catalysed hydroacylation; Rh(I)-catalysed hydrogenation; formic acid; ethene; reaction mechanism; DFT

1. Introduction

Transition metal-catalysed C—H bond activation has received considerable attention in synthetic organic chemistry since the cleavage of an unreactive C—H bond and subsequent addition of the C—H unit to unsaturated substrates such as alkene and alkyne could lead to the formation of a new C—C bond [1–7]. The formation of a C—C bond is one of the most fundamental projects in organic chemistry. Much effort has naturally been devoted to develop more convenient and efficient strategies for the formation of C—C bonds. During the last two decades, many successful applications of catalytic C—H bond activation directed towards the construction of C—C bonds have been reported in synthetic communities [8]. The C—C bond-forming reactions via C—H bond activation have extensively been the focus of study in the fields of organic and organometallic chemistry [7–10].

The rhodium-catalysed intra- and intermolecular hydroacylation (Scheme 1) of alkene or alkyne is one of the most useful C—H bond activation processes [11–20]. The reaction mechanism of rhodium (I)-catalysed hydroacylation of ethene and aldehydes has been studied by our group [21] using density functional theory (DFT; B3LYP). Noyori's group [22–23] studied ruthenium- or rhodium-catalysed hydrogenation of ketone using formic acid. The theoretical data available for the mechanism of rhodium-catalysed hydroacylation and hydrogenation of alkene using formic acid are rather limited, and even the detailed quantum chemical studies are hardly reported. Therefore, in order to understand the reaction mechanism of rhodium-catalysed hydroacylation and hydrogenation of alkene using formic acid in detail, rhodium(I)-catalysed hydroacylation and hydrogenation of ethene using formic acid (Scheme 2) were studied in the present work.

2. Computational methods and models

The present computations were based on rhodium(I)-catalysed hydroacylation and hydrogenation of ethene using formic acid (Scheme 2). All the intermediates and transition states are fully optimised by means of the DFT [24], with Becke's three-parameter functional (B3) [25] and Lee, Yang, and Parr (LYP) correlation energies [26,27]. The basis set 6-311++G(d,p) is for C, O and H, and LANL2DZ is for Rh and P, by adding one set of f-polarisation to rhodium (exponent: 1.350) [28] and one set of d-polarisation to phosphorus (exponent: 0.371) [29], and self-consistent fluids (SCF) convergence criterion is set to 10^{-7}. The vibrational and natural bond orbital (NBO) analyses [30–37] are performed at the same computational level on the basis of the optimised geometries. All the species are positively identified for local minima with zero of the

*Corresponding author. Email: qingxim@sdau.edu.cn

ISSN 0892-7022 print/ISSN 1029-0435 online

DOI: 10.1080/08927020802534843
http://www.informaworld.com

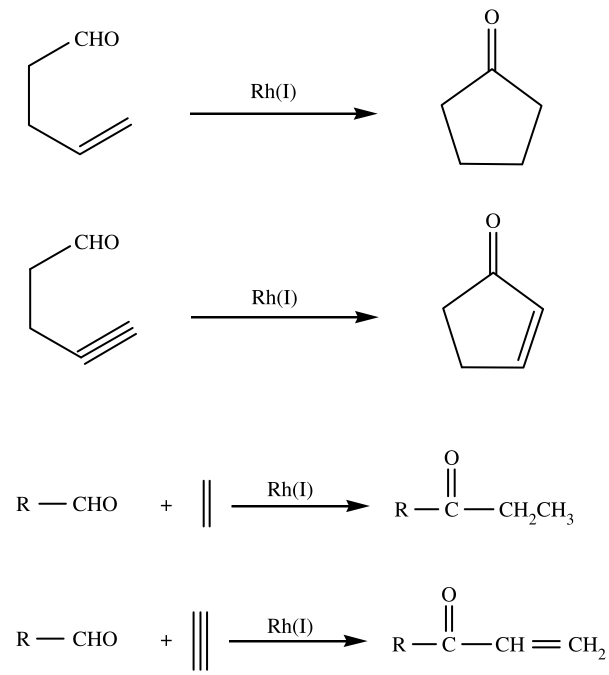

Scheme 1. Rh(I)-catalysed intramolecular and intermolecular hydroacylation.

number of imaginary frequencies and for transition states with the sole imaginary frequency. Transition states are verified by intrinsic reaction coordinate [38] calculations and by animating the negative eigenvector coordinates with a visualisation program (Molekel 4.3) [39–40]. All these computations are carried out using the Gaussian 03 program package [41]. Total electronic energies corrected with zero-point energies (ZPE), E, formation energies, ΔE, reaction energy barriers, $\Delta E^{\neq}$ and total Gibbs free energies corrected with ZPE, G, formation Gibbs free energies, ΔG, reaction Gibbs free energy barriers, $\Delta G^{\neq}$ and the first two vibrational frequencies, ν_1 and ν_2, are summarised in Table 1.

In addition, the electron densities at the bond critical points (BCPs) or the ring critical points (RCPs) for some species are calculated by employing the AIM 2000 program package [42,43].

3. Results and discussion

Possible reaction mechanism of Rh(I)-catalysed hydroacylation and hydrogenation is illustrated in Scheme 3: (1) Rh-catalysed oxidative addition of formic acid, (2) the hydroacylation of ethene (reaction mode 'a', Path 1), (3) the hydroacylation of ethene (reaction mode 'b', Path 2), (4) the hydrogenation of ethene (Path 3) and (5) the hydrogenation of ethene (Path 4).

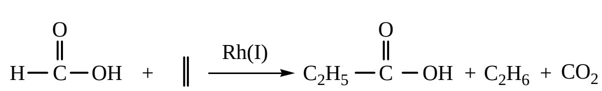

Scheme 2. Rh(I)-catalysed hydroacylation and hydrogenation of C_2H_4 and HCO_2H.

Paths 1 and 2 are the reaction channels of Rh(I)-catalysed hydroacylation: as shown in Figure 1, in **M2**, the attack of H(6) on C(2) is marked by 'a', while the attack of C(5) on C(2) is marked by 'b'. Paths 3 and 4 are the reaction channels of Rh(I)-catalysed hydrogenation, which are marked by 'c'.

3.1 The oxidative addition of formic acid

As shown in Scheme 3, the transfer of H(6) from C(5) to Rh(3) in the complex **M1** leads, via the transition state **TS1**, to the complex **M2**. This reaction step is generally named as the oxidative addition of formic acid.

The optimised structure of Rh(I) complex **M1** is shown in Figures 1 and 2. The four-coordinate rhodium (I) complex is square planar, and Rh—P, Rh—C and Rh—O bonds are about 2.35, 2.24 and 2.21 Å, respectively. As illustrated in the NBO analysis, there is the back-donation π bond between rhodium and π bond of ethene. The occupied π orbital of ethene acts on the empty hybrid orbital of rhodium leading to the σ coordinate bond; on the other hand, the occupied d orbital (d_{xy}, d_{xz}, d_{yz}) of rhodium acts on the empty π^* orbital of ethene leading to the back-donation π bond. Obviously, the formation of the back-donation π bonds lowers the system's energy and makes **M1** more stable.

In the transition states **TS1**, as illustrated in Figure 2, C(5)—H(6) bond is lengthened considerably and Rh(3)—H(6) bond is shortened, compared with those of the complex **M1**. It is clear that there is a significant interaction between Rh(3) and H(6), and C(5)—H(6) bond is weakened greatly, which is demonstrated by analysing the changes in the electron densities $\rho(r)$ of the BCPs and the bond orders P_{ij} (see Table S1, available online, e.g. Rh(3)—H(6) bond, $\rho(r)$, **M1**: 0.000 → **TS1**: 0.130 → **M2**: 0.168 eÅ^{-3}; P_{ij}, **M1**: 0.000 → **TS1**: 0.293 → **M2**: 0.463). It is demonstrated by the present computations that the fracture of C(5)—H(6) bond and the formation of Rh(3)—H(6) bond may be in concurrence. The NBO analysis of **TS1** indicates that Rh(3)—C(5) bond shows strong single-bonded character, and the NBO energies of the bonding orbital $\sigma_{Rh(3)-C(5)}$ is −1330 kJ/mol. Rh(3)—C(5) bond is composed of 59.9% sd$^{1.3}$ hybrid orbital of rhodium and 40.1% sp$^{2.1}$ hybrid orbital of carbon.

The five-coordinate rhodium complex **M2** is a pentahedron structure, and the four ligands (ethene, —CO_2H and two groups PH_3) are almost in the same plane. The complex **M2** has also the back-donation π bond between rhodium and π bond of ethene. The NBO analysis of **M2** indicates that Rh(3)—C(5) and Rh(3)—H(6) bonds show strong single-bonded character, and the NBO energies of the bonding orbitals $\sigma_{Rh(3)-C(5)}$ and

Table 1. Total energies E (× 2625.5 kJ/mol), formation energies ΔE (kJ/mol), reaction energy barriers $\Delta E^{\neq}$(kJ/mol) and total Gibbs free energies G (× 2625.5 kJ/mol), formation Gibbs free energies ΔG (kJ/mol), reaction Gibbs free energy barriers $\Delta G^{\neq}$(kJ/mol) and frequencies (cm^{-1}) for all the compounds.

	E	ΔE	$\Delta E^{\neq}$	G	ΔG	$\Delta G^{\neq}$	ν_1	ν_2
ca	− 125.8574			− 125.8912			16.98	63.49
Ethene	− 78.5648			− 78.5863			834.91	973.68
HCO_2H	− 189.7941			− 189.8182			630.34	679.70
M1	− 394.2900			− 394.3345			36.08	44.47
TS1	− 394.2539		94.78	− 394.2948		104.23	466.89i	43.11
M2	− 394.2646	66.69		− 394.3075	70.89		43.91	58.39
TS2a	− 394.2449		51.72	− 394.2864		55.40	112.67i	33.06
TS2b	− 394.2363		74.30	− 394.2768		80.60	395.06i	50.53
M3a	− 394.2684	− 9.98		− 394.3117	− 11.03		36.80	48.38
M3b	− 394.2946	− 78.77		− 394.3354	− 73.25		47.44	69.12
TS3a	− 394.2406		72.99	− 394.2814		79.55	356.85i	52.83
TS3b	− 394.2850		25.20	− 394.3254		26.25	775.34i	60.57
M4	− 394.3047	− 95.31		− 394.3495	− 99.24		12.89	35.13
		− 26.52			− 37.02			
P1	− 268.3978			− 268.4275			32.77	222.13
TS4c	− 394.2043		158.32	− 394.2467		159.63	1985.08i	20.48
M5c	− 394.2463	48.05		− 394.2899	46.21		37.15	45.20
TS5c	− 394.2116		91.10	− 394.2546		92.68	1372.22i	18.70
M6c	− 205.6473	− 95.04		− 205.6847	− 134.95		59.98	85.11
TS6c	− 205.6412		16.02	− 205.6804		11.29	545.96i	63.87
M7c	− 205.6432	10.76		− 205.6815	8.40		50.90	56.40
TS7c	− 205.6405		7.09	− 205.6780		9.19	690.29i	56.31
CH_3CH_3	− 79.7823			− 79.8054			306.59	825.97
CO_2	− 188.6352			− 188.6566			669.03	669.03
TS8c	− 394.2042		168.56	− 394.2485		165.93	1609.42i	14.05
M8c	− 394.2834	− 39.38		− 394.3295	− 46.73		23.04	24.94
TS9c	− 394.2747		22.84	− 394.3223		18.90	641.43i	9.56

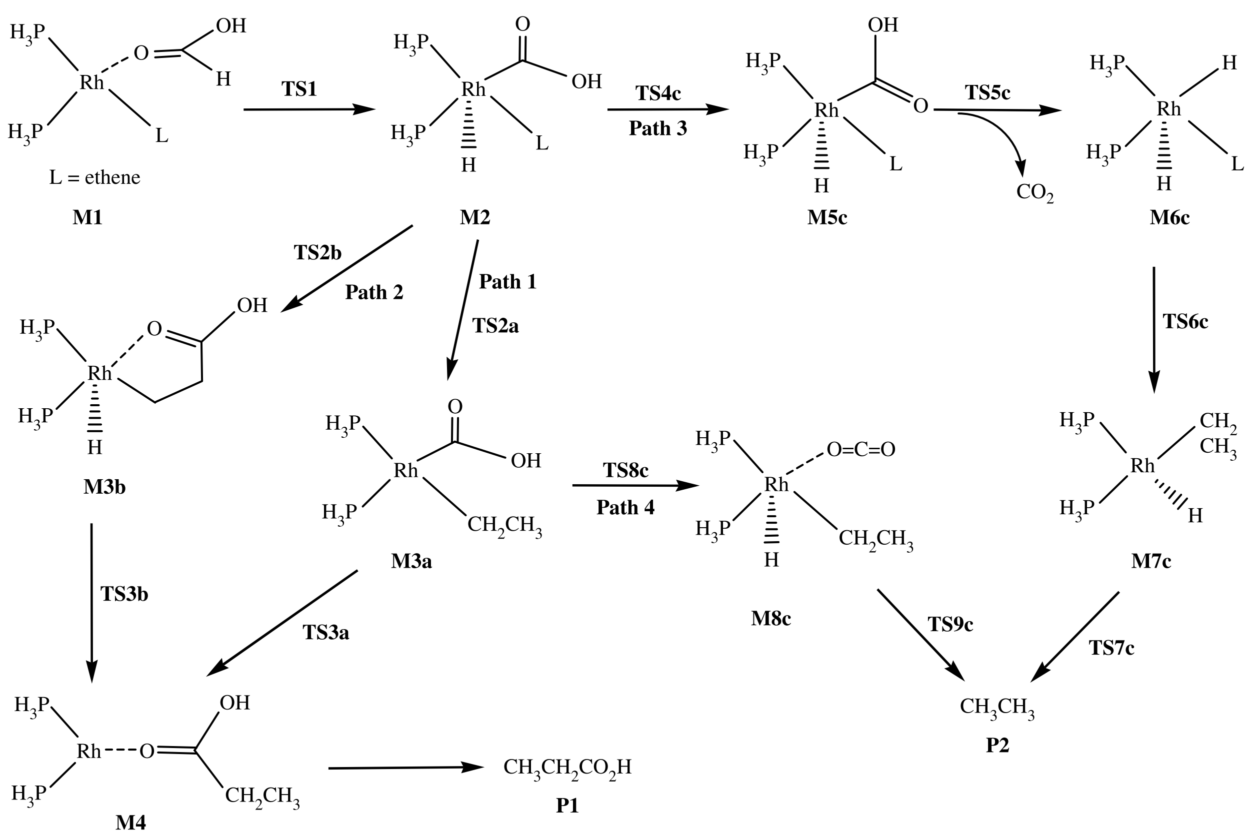

Scheme 3. Possible reaction mechanism of Rh(I)-catalysed hydroacylation and hydrogenation of ethene.

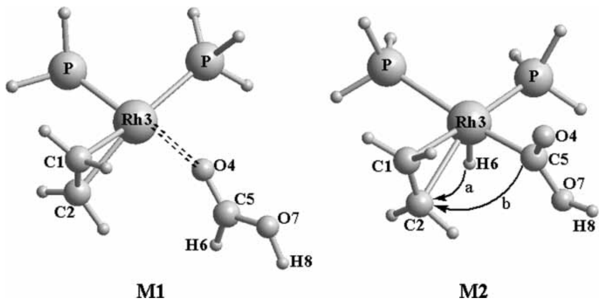

Figure 1. The attack of H(6) in the complex **M2**.

$\sigma_{Rh(3)-H(6)}$ are -1502 and -1283 kJ/mol, respectively, which indicates that Rh(3)—C(5) and Rh(3)—H(6) bonds of **M2** are strengthened relative to those of **TS1**. Rh(3)—C(5) bond is composed of 51.6% $sd^{2.5}$ hybrid orbital of rhodium and 48.4% $sp^{2.1}$ hybrid orbital of carbon; Rh(3)—H(6) bond is composed of 42.1% $sd^{2.3}$ hybrid orbital of rhodium and 57.9% s orbital of hydrogen. The NBO analysis of **M2** also indicates that the NBO energy of π bond orbital of C(1)—C(2) is -1242 kJ/mol, which is much higher than that of ethene (NBO energy of π bond ethene is -2004 kJ/mol). This makes $\pi_{C(1)-C(2)}$ fracture more easier and the attack of C(5) or H(6) on C(2) more possible.

3.2 Path 1 (reaction mode 'a', the hydroacylation of ethene)

As shown in Scheme 3, the transfer of H(6) from Rh(3) to C(2) in the complex **M2** traverses the transition state **TS2a**, and then leads to the complex **M3a**. And then the attack of C(1) on C(5) leads, via the transition state **TS3a**, to the Rh–ketone complex **M4**. The decomposition of the complex **M4** results in the product **P1**.

In the transition state **TS2a**, as illustrated in Figure 2, Rh(3)—H(6) bond is lengthened considerably and

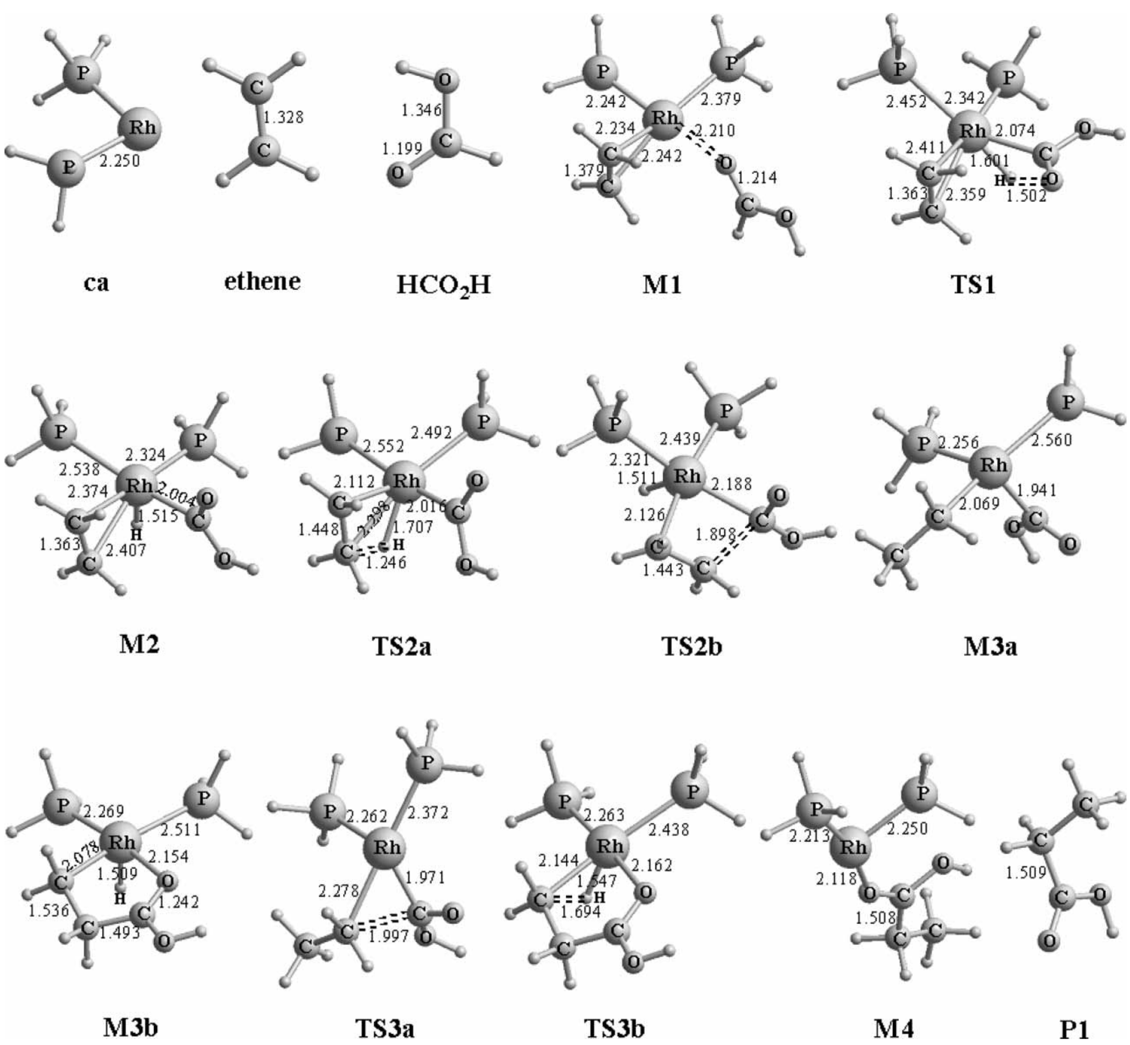

Figure 2. The intermediates and transition states of Rh(I)-catalysed hydroacylation of ethene.

C(2)—H(6) bond is shortened, compared with those in the complex **M2**. These results imply that there is a significant interaction between C(2) and H(6), and the Rh(3)—H(6) bond is weakened greatly, which is demonstrated by analysing the changes in the electron densities $\rho(r)$ of the BCPs and the bond orders P_{ij} (Table S1, e.g. Rh(3)—H(6) bond, $\rho(r)$, **M2**: 0.168 → **TS2a**: 0.096 → **M3a**: 0.000 eÅ^{-3}; P_{ij}, **M2**: 0.463 → **TS2a**: 0.011 → **M3a**: 0.000). It is demonstrated by the present computations that the fracture of Rh(3)—H(6) bond and the formation of C(2)—H(6) bond may be in concurrence. The NBO analysis illustrates that Rh(3)—C(1) and C(2)—H(6) bonds show strong single-bonded character, and the NBO energies are −1339 and −1699 kJ/mol, respectively. Rh(3)—C(1) bond is composed of 64.0% d orbital of rhodium and 36.0% sp$^{11.6}$ hybrid orbital of carbon. C(2)—H(6) bond is composed of 59.0% sp$^{4.2}$ hybrid orbital of carbon and 41.0% s orbital of hydrogen. Transition state **TS2a** involves an Rh(3)—C(1)—C(2)—H(6) four-membered ring and the electron density of the RCP is 0.070 eÅ^{-3}.

The complex **M3a** is of anamorphic tetrahedral structure, and the C(1)—Rh(3)—C(5)—P torsion angle is 90.5°. As illustrated in the NBO analysis, Rh(3)—C(1) bond shows strong single-bonded character, and the NBO energy is −1334 kJ/mol. Rh(3)—C(1) bond is composed of 50.9% sd$^{2.4}$ hybrid orbital of rhodium and 49.1% sp$^{5.7}$ hybrid orbital of carbon. The NBO energy of the bonding orbital $\sigma_{Rh(3)-C(5)}$ is −1589 kJ/mol, and Rh(3)—C(5) bond is composed of 50.3% sd$^{3.0}$ hybrid orbital of rhodium and 49.7% sp$^{2.3}$ hybrid orbital of carbon.

In the transition state **TS3a** (Figure 2), C(1)—C(5) bond is shortened, compared with that of the complex **M3a**. This result implies that there is a significant interaction between C(1) and C(5), which is demonstrated by analysing the changes in the electron densities $\rho(r)$ of the BCPs and the bond orders P_{ij} (Table S1). Transition state **TS3a** involves a C(1)—Rh(3)—C(5) three-membered ring, and the electron density of the RCPs is 0.070 eÅ^{-3}.

3.3 Path 2 (reaction mode 'b', the hydroacylation of ethene)

As shown in Scheme 3, in the complex **M2**, the attack of C(1) on C(5) leads, via the transition state **TS2b**, to the complex **M3b**. And the transfer of H(6) from Rh(3) to C(2) traverses the transition state **TS3b**, and then leads to the complex **M4**. The decomposition of the complex **M4** results in the product **P1**.

In the transition state **TS2b**, C(2)—C(5) bond is shortened, compared with the complex **M2**. This implies that there is a significant interaction between C(2) and C(5), which is demonstrated by analysing the changes in the electron densities $\rho(r)$ of the BCPs and the bond orders P_{ij} (Table S1). The NBO analysis of **TS2b** indicates that Rh(3)—C(1) bond shows strong single-bonded character, and the NBO energies of the bonding orbital $\sigma_{Rh(3)-C(1)}$ is −1170 kJ/mol. Rh(3)—C(1) bond is composed of 53.3% sd$^{2.9}$ hybrid orbital of rhodium and 46.7% sp$^{9.6}$ hybrid orbital of carbon. **TS2a** involves an Rh(3)—C(1)—C(2)—C(5) four-membered ring and the electron density of the RCP is 0.057 eÅ^{-3}. The complex **M3b** is of a pentahedron structure, and involves an Rh(3)—C(1)—C(2)—C(5)—O(4) five-membered ring and the electron density of the RCP is 0.025 eÅ^{-3}. The NBO analysis of **M3b** indicates that Rh(3)—C(1) bond shows strong single-bonded character, and the NBO energies of the bonding orbital $\sigma_{Rh(3)-C(1)}$ is −1290 kJ/mol. Rh(3)—C(1) bond is composed of 46.0% sd$^{2.3}$ hybrid orbital of rhodium and 54.0% sp$^{4.6}$ hybrid orbital of carbon.

In the transition state **TS3b**, Rh(3)—H(6) bond is lengthened considerably and C(1)—H(6) bond is shortened, compared with those of the complex **M3b**. These results imply that there is a significant interaction between C(1) and H(6), and the Rh(3)—H(6) bond is weakened greatly, which is demonstrated by analysing the changes in the electron densities $\rho(r)$ of the BCPs and the bond orders P_{ij} (Table S1). It is demonstrated by the results that the formation of C(1)—H(6) bonds and the fracture of Rh(3)—H(6) bonds may be in concurrence. Similar to the complex **M3b**, transition state **TS3b** also involves an Rh(3)—C(1)—C(2)—C(5)—O(4) five-membered ring and the electron density $\rho(r)$ of the RCP is 0.024 eÅ^{-3}.

As summarised in Table 1, the formation of five-coordinate rhodium complex **M2** is endothermic, and the absorbed Gibbs free energy is 70.89 kJ/mol; nevertheless, the formation of **M3a**, **M3b** and **M4** is exothermic, and the released Gibbs free energies are −11.03, −73.25 and −99.24 or −37.02 kJ/mol, respectively. The reaction Gibbs free energy barrier of the oxidative addition of formic acid is 104.23 kJ/mol, and the reaction Gibbs free energy barriers of **M2 → M3a**, **M3a → M4**, **M2 → M3b** and **M3b → M4** are 55.40, 79.55, 80.60 and 26.25 kJ/mol, respectively. Obviously, the oxidative addition of formic acid is the rate-determining step for Rh(I)-catalysed hydroacylation of ethene. As discussed above, Paths 1 and 2 are the two reaction modes of Rh(I)-catalysed hydroacylation of ethene. And the reactions **M2 → M3a** and **M3b → M4** are H-transfer reactions; the reactions **M3a → M4** and **M2 → M3b** are the C—C bond-forming reactions. It is clear that the reaction energy barriers of the H-transfer reaction are lower than those of the C—C bond-forming reaction. Therefore, the H-transfer reaction is prior to the C—C bond-forming reaction, and thus the reaction mode 'a' (i.e. **ca → M1 → TS1 → M2 → TS2a → M3a → TS3a → M4 → P1**) is the dominant reaction pathway for Rh(I)-catalysed hydroacylation of ethene.

3.4 Path 3 (the hydrogenation of ethene)

As shown in Scheme 3, in the complex **M2**, the transfer of H(8) from O(7) to O(4) leads to the complex **M5c**, which is an isomer of the complex **M2**, and the corresponding transition state is **TS4c**. (Therefore, this reaction step is generally named the isomerisation of five-coordinate rhodium(I) complex **M2**.) The transfer of H(8) from O(4) to Rh(3) in **M5c** traverses the transition state **TS5c** leading to the complex **M6c** and CO_2. And then there occurs the hydrogenation of ethene generating ethane (**P2**) via two reaction steps of hydrogen transfer reaction (**M6c** → **TS6c** → **M7c** → **TS7c** → **P2**).

TS4c is the transition state of the transfer of H(8) from O(7) to O(4) in **M2**, and it involves an O(4)—C(5)—O(7)—H(8) four-membered ring, and the electron density $\rho(r)$ of the RCP is $0.104\,\mathrm{e\AA^{-3}}$. The complex **M5c** is similar to **M2**, and both of them are pentahedron structures (Figure 3).

In the transition state **TS5c**, as shown in Figure 3, Rh(3)—H(8) and O(4)—C(5) bonds are shortened and Rh(3)—C(5) and O(4)—H(8) bonds are lengthened, compared with those of **M5c**. These results imply that Rh(3)—H(8) and O(4)—C(5) bonds are strengthened, and Rh(3)—C(5) and O(4)—H(8) bonds are weakened, which is demonstrated by analysing the changes in the electron densities $\rho(r)$ of the BCPs and the bond orders P_{ij} (Table S1). It is demonstrated by the results that the formation of Rh(3)—H(8) and $\pi_{O(4)-C(5)}$ bonds and the fracture of Rh(3)—C(5) and O(4)—H(8) bonds may be in concurrence. There is an Rh(3)—C(5)—O(4)—H(8) four-membered ring, and the electron density $\rho(r)$ of the RCP is $0.041\,\mathrm{e\AA^{-3}}$. Similar to **M2** and **M5c**, the five-coordinate complex **M6c** is a pentahedron structure, and the four ligands (ethene, hydrogen and two groups PH_3) are almost in the same plane.

TS6c and **TS7c** are the two transition states of two reaction steps of the hydrogenation of ethene generating

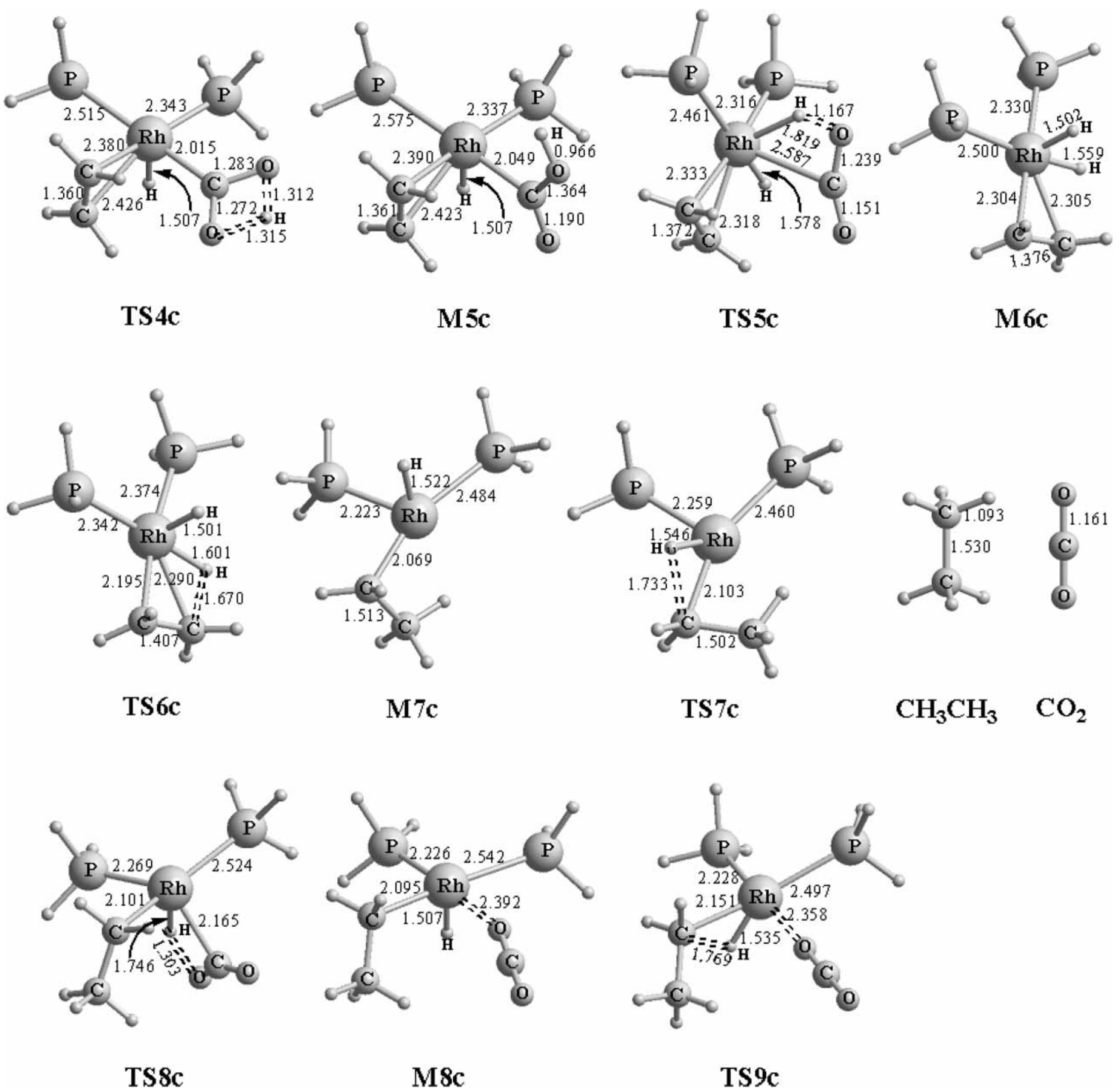

Figure 3. The intermediates and transition states of Rh(I)-catalysed hydrogenation of ethene.

ethane. There is an Rh(3)—C(1)—C(2)—H four-membered ring in **TS6c**, and the electron density $\rho(r)$ of the RCP is 0.069 eÅ^{-3}.

As summarised in Table 1, the formation of the complexes **M5c** and **M7c** are endothermic, and the absorbed Gibbs free energies are 46.21 and 8.40 kJ/mol, respectively; nevertheless, the formation of **M6c** is exothermic, and the released Gibbs free energy is −134.95 kJ/mol. The reaction Gibbs free energy barriers of **M2 → M5c**, **M5c → M6c**, **M6c → M7c** and **M7c → P2** are 159.63, 92.68, 11.29 and 9.19 kJ/mol, respectively. Obviously, the reaction Gibbs free energy barrier of **M2 → M5c** is the biggest, which is much bigger than that of the oxidative addition of formic acid. Therefore, the formation of the complex **M5c** is the rate-determining step for Path 3 (Rh(I)-catalysed hydrogenation of ethene).

3.5 *Path 4 (the hydrogenation of ethene)*

As shown in Scheme 3, in the complex **M3a**, the transfer of H(8) from O(4) to Rh(3) leads, via the transition state **TS8c**, to the complex **M8c**, and then traverses the transition state **TS9c** resulting in ethane and carbon dioxide.

TS8c involves an Rh(3)—C(5)—O(7)—H(8) four-membered ring, and the electron density $\rho(r)$ of the RCP is 0.067 eÅ^{-3}. The five-coordinate complex **M8c** is a pentahedron structure, and the four ligands (—Et, CO_2, and two groups PH_3) are almost in the same plane, and Rh(3)—H(8) bond shows strong single-bonded character, and the NBO energy of the bonding orbital $\sigma_{Rh(3)-H(8)}$ is −1294 kJ/mol.

TS9c is the transition state of the transfer of H(8) from Rh(3) to C(1). The hydrogen transfer reaction makes Rh(3)—C(1) and Rh(3)—H(8) bonds fracture and leads to ethane.

As summarised in Table 1, the formation of **M8c** is exothermic, and the released Gibbs free energy is −46.73 kJ/mol. The reaction Gibbs free energy barriers of **M3a → M8c** and **M8c → P2** are 165.93 and 18.90 kJ/mol, respectively. Obviously, the reaction Gibbs free energy barrier of **M3a → M8c** is bigger, which is much bigger than that of the oxidative addition of formic acid. Therefore, the formation of the complex **M8c** is the rate-determining step for Path 4 (Rh(I)-catalysed hydrogenation of ethene).

3.6 *Overview of the mechanism*

As discussed above, Paths 1 (**ca → M1 → TS1 → M2 → TS2a → M3a → TS3a → M4 → P1**) and 2 (**ca → M1→ TS1 → M2 → TS2b → M3b → TS3b → M4 → P1** are the two reaction pathways of Rh(I)-catalysed hydroacylation of ethene; Paths 3 (**ca → M1 → TS1 → M2 → TS4c → M5c → TS5c → M6c → TS6c → M7c → TS7c → P2**) and 4 (**ca → M1 → TS1 → M2 → TS2a → M3a → TS8c → M8c → TS7c → P2**) are the two reaction pathways of Rh(I)-catalysed hydrogenation of ethene. Figure 4 illustrates the DFT energy relationship for Rh(I)-catalysed hydroacylation and hydrogenation of ethene. Rh(I)-catalysed hydroacylation of ethene is exothermic, and the released Gibbs free energy is −60.39 kJ/mol. And Rh(I)-catalysed hydrogenation of ethene is also exothermic, and the released Gibbs free energy is −150.97 kJ/mol.

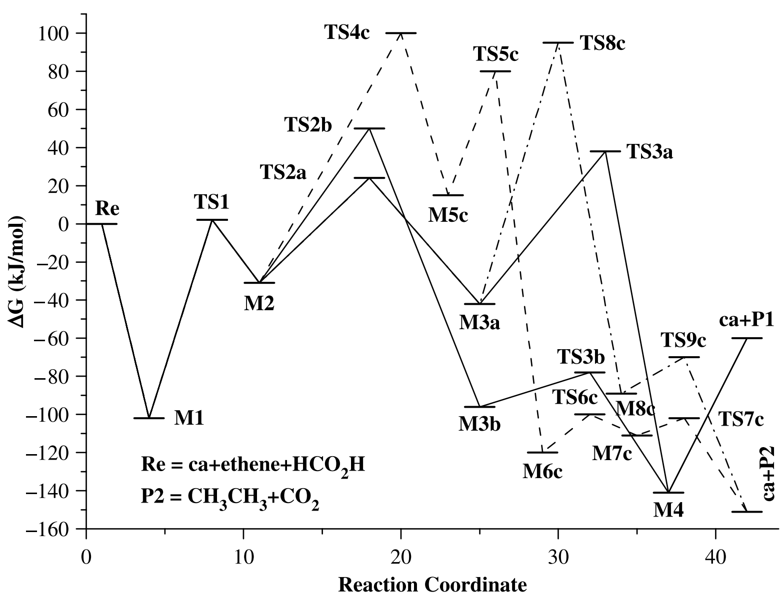

Figure 4. Energy relationship for Rh(I)-catalysed hydroacylation and hydrogenation of ethene.

The oxidative addition of formic acid is the rate-determining step for Rh(I)-catalysed hydroacylation of ethene (Paths 1 and 2). The formation of the complex **M5c** is the rate-determining step for Path 3. The formation of the complex **M8c** is the rate-determining step for Path 4. Because the reaction energy barrier of the oxidative addition of formic acid is lower than that of **M2 → M5c** and **M3a → M8c**, Rh(I)-catalysed hydroacylation of ethene is more dominant than Rh(I)-catalysed hydrogenation of ethene. In Rh(I)-catalysed hydroacylation of ethene, the H-transfer reaction is prior to the C—C bond-forming reaction. Therefore, the reaction mode 'a' (i.e. **ca → M1 → TS1 → M2 → TS2a → M3a → TS3a → M4 → P1**) is the dominant reaction pathway for Rh(I)-catalysed hydroacylation and hydrogenation of ethene. The dominant product is **P1** (propane acid).

4. Conclusion

In this study, we have investigated Rh(I)-catalysed hydroacylation and hydrogenation of ethene with formic acid. All the intermediates and the transition states were optimised completely at the B3LYP/6-311++G(d,p) level (LANL2DZ(d) for Rh, P). The oxidative addition of formic acid is the rate-determining step for Rh(I)-catalysed hydroacylation of ethene. The formation of the complexes **M5c** (for Path 3) and **M8c** (for Path 4) are the rate-determining steps for Rh(I)-catalysed hydrogenation of ethene. Rh(I)-catalysed hydroacylation of ethene is the dominant reaction mode for Rh(I)-catalysed hydroacylation and hydrogenation of ethene with formic acid. In Rh(I)-catalysed hydroacylation of ethene, the H-transfer reaction is prior to the C—C bond-forming reaction. Therefore, the reaction mode 'a' (Path 1) is the dominant reaction pathway for Rh(I)-catalysed hydroacylation and hydrogenation of ethene. The theoretically predicted dominant product is propane acid.

References

[1] C. Jun and J.H. Lee, *Application of C—H and C—C bond activation in organic synthesis*, Pure. Appl. Chem. 76 (2004), pp. 577–587.
[2] C. Jia, T. Kitamura, and Y. Fujiwara, *Catalytic functionalization of arenes and alkanes via C—H bond activation*, Acc. Chem. Res. 34 (2001), pp. 633–639.
[3] F. Kakiuchi and S. Murai, *Activation of C—H bonds: catalytic reactions*, Top. Organomet. Chem. 3 (1999), pp. 47–79.
[4] Y. Guari, S. Sabo-Etienne, and B. Chaudret, *Catalytic formation of carbon—carbon bonds by activation of carbon—hydrogen bonds*, Eur. J. Inorg. Chem. 1999 (1999), pp. 1047–1055.
[5] B.A. Arndtsen, R.G. Bergman, A. Mobley, and T.H. Peterson, *Selective intermolecular carbon—hydrogen bond activation by synthetic metal complexes in homogeneous solution*, Acc. Chem. Res. 28 (1995), pp. 154–162.
[6] A.E. Shilov and G.B. Shul′pin, *Activation of C—H bonds by metal complexes*, Chem. Rev. 97 (1997), pp. 2879–2932.
[7] G. Dyker, *Transition metal catalyzed coupling reactions under C—H activation*, Angew. Chem. Int. Ed. 38 (1999), pp. 1698–1712.
[8] V. Ritleng, C. Sirlin, and M. Pfeffer, *Ru-, Rh-, and Pd-catalyzed C—C bond formation involving C—H activation and addition on unsaturated substrates: reactions and mechanistic aspects*, Chem. Rev. 102 (2002), pp. 1731–1770.
[9] J.A. Labinger and J.E. Bercaw, *Understanding and exploiting C—H bond activation*, Nature 417 (2002), pp. 507–514.
[10] F. Kakiuchi and S. Murai, *Catalytic C—H/olefin coupling*, Acc. Chem. Res. 35 (2002), pp. 826–834.
[11] S.-I. Inoue, H. Takaya, K. Tani, S. Otsuka, T. Sato, and R. Noyori, *Mechanism of the asymmetric isomerization of allylamines to enamines catalyzed by 2,2′-bis(diphenylphosphino)-1,1′binaphthyl-rhodium complexes*, J. Am. Chem. Soc. 112 (1990), pp. 4897–4905.
[12] S.H. Bergens and B. Bosnich, *Homogeneous catalysis. Catalytic production of simple enols*, J. Am. Chem. Soc. 113 (1991), pp. 958–967.
[13] R.W. Barnhart, X.-Q. Wang, P. Noheda, S.H. Bergens, J. Whelan, and B. Bosnich, *Asymmetric catalysis. Asymmetric catalytic intramolecular hydroacylation of 4-pentenals using chiral rhodium diphosphine catalysts*, J. Am. Chem. Soc. 116 (1994), pp. 1821–1830.
[14] C.-H. Jun, J.-B. Hong, and D.-Y. Lee, *Chelation-assisted hydroacylation*, Synlett (1999), pp. 1–12.
[15] A.D. Aloise, M.E. Layton, and M.D. Shair, *Synthesis of cyclooctenones using intramolecular hydroacylation*, J. Am. Chem. Soc. 122 (2000), pp. 12610–12611.
[16] C.-H. Jun, J.-H. Chung, D.-Y. Lee, A. Loupy, and S. Chatti, *Solvent-free chelation-assisted intermolecular hydroacylation: effect of microwave irradiation in the synthesis of ketone from aldehyde and 1-alkene by Rh(I) complex*, Tetrahedron. Lett. 42 (2001), pp. 4803–4805.
[17] K. Tanaka and G.C. Fu, *A versatile new method for the synthesis of cyclopentenones via an unusual rhodium-catalyzed intramolecular trans hydroacylation of an alkyne*, J. Am. Chem. Soc. 123 (2001), pp. 11492–11493.
[18] M.C. Willis and S. Sapmaz, *Intermolecular hydroacylation of acrylate esters: a new route to 1,4-dicarbonyls*, Chem. Commun. (2001), pp. 2558–2559.
[19] C.-H. Jun, C.W. Moon, and D.-Y. Lee, *Chelation-assisted carbon—hydrogen and carbon—carbon bond activation by transition metal catalysts*, Chem. Eur. J. 8 (2002), pp. 2422–2428.
[20] K. Tanaka and G.C. Fu, *Parallel kinetic resolution of 4-alkynals catalyzed by Rh(I)/Tol-BINAP: synthesis of enantioenriched cyclobutanones and cyclopentenones*, J. Am. Chem. Soc. 125 (2003), pp. 8078–8079.
[21] F. Wang, Q. Meng, and M. Li, *Density functional computations of Rh(I)-catalyzed hydroacylation of acetic aldehyde and ethene*, Mol. Sim. 34 (2008), pp. 515–523.
[22] A. Fujii, S. Hashiguchi, N. Uematsu, T. Ikariya, and R. Noyori, *Ruthenium(II)-catalyzed asymmetric transfer hydrogenation of ketones using a formic acid–triethylamine mixture*, J. Am. Chem. Soc. 118 (1996), pp. 2521–2522.
[23] R. Noyori and S. Hashiguchi, *Asymmetric transfer hydrogenation catalyzed by chiral ruthenium complexes*, Acc. Chem. Res. 30 (1997), pp. 97–102.
[24] R.G. Parr and W. Yang, *Density-functional theory of atoms and molecules*, Oxford University Press, New York, NY, 1989.
[25] A.D. Becke, *Density-functional thermochemistry. III. The role of exact exchange*, J. Chem. Phys. 98 (1993), pp. 5648–5652.
[26] C. Lee, W. Yang, and R.G. Parr, *Development of the Colle–Salvetti correlation-energy formula into a functional of the electron density*, Phys. Rev. B 37 (1988), pp. 785–789.
[27] B. Miehlich, A. Savin, H. Stoll, and H. Preuss, *Results obtained with the correlation energy density functionals of Becke and Lee, Yang and Parr*, Chem. Phys. Lett. 157 (1989), pp. 200–206.
[28] A. Höllwarth, M. Böhme, S. Dapprich, A.W. Ehlers, A. Gobbi, K.F. Köhler, R. Stegmann, A. Veldkamp, and G. Frenking, *A set of d-polarization functions for pseudo-potential basis sets of the main group elements Al—Bi and f-type polarization functions for Zn, Cd, Hg*, Chem. Phys. Lett. 208 (1993), pp. 237–240.
[29] A.W. Ehlers, M. Böhme, S. Dapprich, A. Gobbi, A. Höllwarth, V. Jonas, K.F. Köhler, R. Stegmann, A. Veldkamp, and G. Frenking, *A set of f-polarization functions for pseudo-potential basis sets of the*

transition metals Sc—Cu, Y—Ag and La—Au, Chem. Phys. Lett. 208 (1993), pp. 111–114.

[30] E.D. Glendening, A.E. Reed, J.E. Carpenter, F. Weinhold, *NBO Version 3.1*.

[31] J.E. Carpenter and F. Weinhold, *Analysis of the geometry of the hydroxymethyl radical by the 'different hybrids for different spins' natural bond orbital procedure*, J. Mol. Struct. (Theochem.) 169 (1988), pp. 41–62.

[32] J.P. Foster and F. Weinhold, *Natural hybrid orbitals*, J. Am. Chem. Soc. 102 (1980), pp. 7211–7218.

[33] A.E. Reed and F. Weinhold, *Natural bond orbital analysis of near-Hartree–Fock water dimmer*, J. Chem. Phys. 78 (1983), pp. 4066–4073.

[34] A.E. Reed and F. Weinhold, *Vibrational–rotational energy transfer in collisions of HF (*v = *4,* J = *20) with rare gases*, J. Chem. Phys. 78 (1983), pp. 1736–1740.

[35] A.E. Reed, R.B. Weinstock, and F. Weinhold, *Natural population analysis*, J. Chem. Phys. 83 (1985), pp. 735–746.

[36] A.E. Reed, L.A. Curtiss, and F. Weinhold, *Intermolecular interactions from a natural bond orbital, donor–acceptor viewpoint*, Chem. Rev. 88 (1988), pp. 899–926.

[37] F. Weinhold and J.E. Carpenter, in *The structure of small molecules and ions,* R. Naaman and Z. Vager, eds., Plenum, New York, NY, 1988, pp. 227–236.

[38] C. Gonzalez and H.B. Schlegel, *Reaction path following in mass-weighted internal coordinates*, J. Phys. Chem. 94 (1990), pp. 5523–5527.

[39] P. Flükiger, H.P. Lüthi, S. Portmann, and J. Weber, *MOLEKEL 4.3*, Swiss Center for Scientific Computing, Manno, Switzerland, 2000–2002.

[40] S. Portmann and H.P. Lüthi, *MOLEKEL: an interactive molecular graphics tool*, Chimia 54 (2000), pp. 766–770.

[41] M.J. Frisch, G.W. Trucks, H.B. Schlegel, G.E. Scuseria, M.A. Robb, J.R. Cheeseman, J.A. Montgomery, J.T. Vreven, K.N. Kudin, J.C. Burant, et al., *Gaussian 03. Revision B.03*, Gaussian, Inc., Pittsburgh, PA, 2003.

[42] R.F.W. Bader, *Atoms in Molecules, A quantum Theory; International Series of Monographs in Chemistry*, vol. 22, Oxford University Press, Oxford, UK, 1990.

[43] F. Biegler-König, J. Schönbohm, R. Derdau, D. Bayles, and R.F.W. Bader, *AIM 2000. Version 1*, 2000.